Eco-friendly polymer succinate capping on silver nano-particles for enhanced stability: a UV-Vis and electrochemical particle impact study

Azhar Abbas [1,2,*], Hatem M. A. Amin [1,5], Muhammad Akhtar [3,4], Muhammad A. Hussain[2], Christopher Batchelor-McAuley[1], Richard G. Compton [1]

1- Oxford University, Department of Chemistry, Physical and Theoretical Chemistry Laboratory, South Parks Road, Oxford, OX1 3QZ, United Kingdom

2- University of Sargodha, Department of Chemistry, Ibne Sina Block, Sargodha 40100, Pakistan

3- Islamia University of Bahawalpur, Faculty of Pharmacy and Alternative Medicine, Department of Pharmacy, Bahawalpur 63100, Pakistan.

4- King's College London, Faculty of Life Sciences & Medicine, School of Cancer and Pharmaceutical Sciences, London, SE1 9NH, United Kingdom.

5- Cairo University, Faculty of Science, Department of Chemistry, Giza, 12613 Egypt

Azhar Abbas: azharabbas73@yahoo.com
Hatem M. A. Amin: hatem@pc.uni-bonn.de
Muhammad Akhtar: muhammad.akhtar@iub.edu.pk
Muhammad A. Hussain: majaz172@yahoo.com
Christopher Batchelor-McAuley: christopher.batchelor-mcauley@chem.ox.ac.uk
Richard G. Compton: richard.compton@chem.ox.ac.uk

[*]Azhar Abbas: azhar.abbas@chem.ox.ac.uk; azharabbas73@yahoo.com

Phone: +44 (0) 7448775793

ABSTRACT

A facile green method is used to synthesize silver nanoparticles (Ag Nps) in one minute. The colloidal stability of two types of Ag Nps (namely, hydroxypropylcellulose-succinate (HPC-Suc) capped silver nanoparticles (Ag Nps@suc) and citrate-capped silver nanoparticles (Ag Nps@cit)) is investigated using UV-Vis spectrometry and electrochemical particle impacts "nano-impacts" measurements. Ag Nps@suc were newly synthesized by simply mixing aqueous solutions of HPC-Suc and silver nitrate and exposure to sunlight. The growth of Ag Nps was controlled by adjusting the exposure time to sun light. Local surface plasmon resonance (LSPR) study was conducted using UV-Vis spectrophotometer. The surface morphology, size, elemental analysis and composition of Ag NPs@suc was determined by SEM-EDX, while ATR-FTIR was used to assess any type of chemical reactions between the precursors. For stability and size distribution measurements zeta-potential (ZP), dynamic light scattering (DSL) and anodic particle coulometry (APC) were performed. The as-prepared Ag Nps@suc exhibited a narrow size distribution with an average diameter of 20 nm. Nps sizing using particles electrochemical impacts method is consistent with SEM and DLS techniques. The results show that Ag Nps@cit are prone to relatively rapid clustering upon addition of electrolyte (100 mM K_2SO_4). On the other hand, Ag Nps@suc exhibit excellent stability with only ~ 9% decay in absorbance over 24 h even at high electrolyte concentration. Using KCl, KBr and NaCl electrolytes, the stability of the synthesized Ag Nps@suc also compares favorably to Ag Nps@cit.

Keywords: Silver nanoparticles, Succinate capping agent, Nanoparticle stability, UV-Vis spectrometry, Nanoparticle-electrode impact

Introduction

There are numerous nano-enabled products of silver in the market, *e.g.*, sportswear, medical implants, bioimaging, biosensors *etc*., which make use of increased catalytic activity (Amin et al., 2015; Amin et al., 2017), electrical conductivity (Hayward et al., 2000; Shipway et al., 2000; Shamaila et al., 2016), anticancer (Mfouo-Tynga et al., 2014; Zhao et al., 2014) and antibacterial characteristics of Ag Nps (Khan et al., 2014) as compared with bulk silver.

Ag Nps undergo several changes such as aggregation, agglomeration, dissolution or surface adsorption. The occurrence of the reaction depends on nanoparticles properties and their local environment (Baalousha, 2017; Peijnenburg et al., 2015). These changes in structure and chemical properties will influence the particle transport, diffusion, reactivity and toxicity (Afshinnia et al., 2017). Clustering (agglomeration and/or aggregation) of Nps reduces their opportunity of uptake into biological systems (Jang et al., 2014). Conversely, increased stability of aqueous dispersions of the Ag Nps may increase environmental persistence (Stuart et al., 2013). For instance, the stability of Ag Nps has been shown to be a crucial factor for their long-term antimicrobial durability (Korshed et al., 2018). Laser generated Ag Nps show 10 days longer activity as compared to chemically modified Ag Nps when tested for an air exposure of 45-days (Korshed et al., 2018).

Different capping agents including natural compounds are used to stabilize Ag Nps (Banach and Pulit-Prociak, 2017). The nature of capping agent affects the size and appearance of the NPs and their interaction with solvent (Raveendran et al., 2003). Therefore, capping agent plays a vital role in the nanoparticle synthesis process.

Carboxylic acid based capping agents are widely used for the capping of Nps because carboxyl groups are recognized as active functional groups for reducing Ag^+ (Bastús et al., 2014). Moreover, carboxylic acids are known to coordinate effectively to Ag Nps (Xie et al., 2007). Among all carboxylic acid capping agents, citrate reduction of silver ions remains the overwhelmingly most popular method to quickly form citrate capped silver nanoparticles (Ag Nps@cit) (Bastús et al., 2014). However, a significant drawback of the Ag Nps@cit is their low stability in electrolyte solutions (Huynh and Chen, 2011).

Nanoparticles stabilized by polymers carrying functional groups are relatively stable (Richard et al., 1991). Coordination of the hydroxyl group of polyethylene glycol (PEG) and polyvinyl alcohol (PVA) to Ag Nps is relatively less effective as compared to carboxylic acids and this limits their use as stabilizing and capping agent (Luo et al., 2005). Polymers carrying carboxylic acid functional groups may be employed to synthesize stable Ag Nps with enhanced stability. The carboxylic acid functional group has

been widely exploited for surface modification of cellulose based polymers (Abbas et al., 2015). Recently, AgNps were developed from a soy protein that contains a large number of hydroxyl groups and has been used as capping and reducing agent, employing one-pot solid state method (Abdelgawad et al., 2017). The hydroxyl groups can help the co-ordination of Ag^+ to the molecular matrix. COOH groups can easily be built on to polysaccharides such as hydroxypropyl cellulose (HPC) by esterification using cyclic anhydrides (*e.g.*, succinic anhydride) (Abbas et al., 2015). These carboxylated polymers are expected to have high attachment of succinate groups which might be exploited for the reduction of Ag^+ to form stable metal Nps. Moreover, if COOH carrying polysaccharides are used to prepare and to cap nanoparticles, their resulting surfaces will also be capped with polysaccharide chains *via* succinate linkers which may further stabilize the formed nanoparticles *via* surface adsorption.

In this study, we evaluate the stability of novelly-synthesized hydroxypropyl cellulose succinate (HPC-Suc) capped Ag Nps using UV-Vis and nano-impacts against agglomeration/aggregation. Herein, nano-impacts is based on anodic particle coulometry (APC) approach which is used to size metal nanoparticles by oxidizing them upon collision with a micro electrode. The as-synthesized Ag Nps@suc were characterized using different spectroscopic and electrochemical techniques. UV-Vis and nano-impacts results revealed significant and useful enhancement in stability of Ag Nps@suc compared to that of Ag Nps@cit. Based on the natural origin of the used cellulose-containing reducing and capping agent, our method can be described as eco-friendly and could have further emerging applications.

Experimental

Materials

Hydroxypropyl cellulose (HPC) (3.46 moles of hydroxypropyl per mole of glucose unit) was provided by a Chinese company, Nanjing Yeshun Industry and International Trading Co. Ltd. Before use it was vacuum dried at 110°C for 5 h. Succinic anhydride was acquired from Fluka. All solvents used were of analytical grade. Silver nitrate, potassium chloride, sodium chloride, potassium sulphate and potassium bromide having maximum reported purity were purchased from Sigma Aldrich. All solutions were prepared with deionized water (18.2 MΩ cm resistivity at 25°C). Spherical citrate capped Ag Nps (Ag Nps@cit) of about 20 nm diameter were synthesized and characterized as previously reported (Lees et al., 2013).

Synthesis of hydroxypropyl cellulose-succinate-capped silver nanoparticles (Ag Nps@suc)

Hydroxypropyl cellulose succinate (HPC-Suc) was synthesized as reported (Abbas et al., 2015). HPC-Suc (100 mg) was dissolved in 10 mL of deionized water (10 mL) and added to 50 mM $AgNO_3$ aqueous solution (10 mL) in the dark. The resultant mixture was then kept in sunlight and progress of the reaction was checked periodically using UV-Vis spectrophotometer. Over a period of 25 min of exposure to sunlight the color of the solution was turned from colorless to light yellow and then to dark brown (Figure 1). This color change is attributed to the formation of Ag Nps@suc of different sizes. The solution was centrifuged for 30 min at 4400 rpm after exposure to sunlight for 60 s and the supernatant containing some unreacted material was removed, leaving solid Ag Nps@suc at the bottom of a falcon tube. Deionized water was added to the tube and centrifuged further for 30 min at 4400 rpm in order to remove any unreacted material. This washing was carried out twice. After washing, solid sample of Ag Nps@suc was isolated and 15 mL of deionized water was added to solid Ag Nps@suc and sonicated for 15 min. This gave a suspension of Ag Nps@suc which was used as a stock for additional studies. This suspension was analysed for quantitation using UV-Vis spectrophotometer (Ngamchuea et al., 2017). The synthesized Ag Nps@suc were also characterized using ATR-FTIR, SEM-EDX, DLS, ZP measurements and impact electrochemistry.

Characterization of Ag Nps@suc

UV-Vis spectrophotometry

UV-Vis experiments were carried out with a Shimadzu UV-1800 spectrophotometer in high precision quartz cells (Hellma Analytics, Germany) having an optical path length of 10 mm. A baseline correction was made with empty cells inside the instrument prior to each experiment. The absorbance was recorded from 300-800 nm. 12 pM solution of Ag Nps@suc and Ag Nps@cit were used to record the UV-Vis spectra.

Stabilities of the Ag Nps@suc and Ag Nps@cit in different electrolytes solutions

UV-Vis experiments (300-800 nm) were also carried out to study the stabilities of 4 pM and 12 pM of Ag Nps@suc and Ag Nps@cit, respectively each in 2 mM, 20 mM and 100 mM of KCl, KBr, NaCl or K_2SO_4 electrolyte solutions over a period of 24 h.

SEM-EDX characterization

High-resolution SEM equipped with EDX (Zeiss Merlin Field Emission Gun (FEG)-SEM) was used to probe the morphology, size, elemental analysis and composition of Ag Nps@suc. The SEM-EDX images were recorded at 5 kV acceleration voltage. As a substrate for the SEM sample, a glassy carbon (GC) plate was used. Previously, the GC plate was immersed in aqua-regia and then was rinsed with nanopure water followed by mechanical polishing with successively smaller diameter alumina powder (1.0 µm, 0.3 µm and 0.05 µm; Buehler, USA) slurries with nanopure water on lapping pads (Buehler, USA). Area calculations and particle size analysis were carried out by ImageJ software.

ATR-FTIR characterization

FTIR spectra of HPC, HPC-Suc and Ag Nps@suc were recorded using a FTIR spectrometer (IRAffinity-1S, SHIMADZU, Japan) equipped with a diamond ATR device (SHIMADZU). FTIR measurements were performed in the range of 400–4000 cm^{-1}. Each spectrum represents an average of 20 scans with 2 cm^{-1} resolution to increase the signal to noise ratio.

DLS and ZP measurements

In order to determine the hydrodynamic diameter, ZP and the stability of the nanoparticles (Ag Nps@suc and Ag Nps@cit), a Malvern Zetasizer Nano ZS was used. The measurements were done using a 633 nm He-Ne laser. To remove any solid contaminants the sample suspension was filtered using Whatman 0.2 µm filter. The filtered sample was hold in a solvent-resistant micro cuvette with a path length of 10 mm. Every sample was equilibrated at 25°C for 2 min in instrument before analysis. Three sets of 12 light scattering measurements were recorded and results were presented as mean ± SD. To measure ZP, AgNPs suspension was placed in disposable folded capillary cells. The Zetasizer software from Malvern was used to analyze the data.

Nano-impacts

A three-electrode arrangement was used in all electrochemical experiments. The cell and the electrodes were placed in a thermally controlled Faraday cage at 25°C. A home-built low noise potentiostat was used to carry out nano-impact experiments. The analog signal was filtered and digitized at a rate of 50 kHz by applying two cascaded RC filters of 100 Hz. This was followed by digital filtering using a four pole Bessel filter (100 Hz). The equipment was validated for the total charge transferred in an impact event (Batchelor-McAuley et al., 2015; Kätelhön et al., 2016). These experiments were performed using a carbon microdisc of 33 µm diameter (IJ Cambria Scientific Ltd, UK) serving as the working

electrode and a leakless Ag/AgCl (in 3.4 M KCl, eDAQ) as a reference electrode while a platinum wire was used as a counter electrode. For sizing the Ag Nps@suc, current-time measurements were performed using a 12 pM solution of Ag Nps@suc in 20 mM KCl by holding the working electrode at 0.8 V against leakless Ag/AgCl for 50 s per scan. In addition to the chronoamperometry experiments, cyclic voltammetry was also carried out to calculate diameter of Ag Nps@suc using the same concentration of Ag Nps@suc (12 pM solution of Ag Nps@suc in 20 mM KCl) at a scanning rate of 50 mV per second. Nano-impact spikes collected from both chronoamperometric and cyclic voltammetric experiments were identified and analyzed to calculate the charge using SignalCounter software developed by Dario Omanovic (Croatia). In order to have an insight into agglomeration state of AgNps, nano-impact experiments were carried out with 12 pM solution of Ag Nps@suc or Ag Nps@cit each in 100 mM K_2SO_4 by holding the working electrode at 0.8 V against leakless Ag/AgCl for 50 s per scan over a time of solution for 3 h.

Results and Discussion

This section reports the synthesis and characterization of Ag Nps@suc. The synthesized Ag Nps@suc were evaluated using the techniques including UV-Vis, SEM-EDX, DLS and ZP, ATR-FTIR and nano-impacts. The clustering of Ag Nps@suc and Ag Nps@cit was investigated using UV-Vis spectrophotometry and nano-impacts in K_2SO_4. This section also reports the stabilities of both types of Nps studied in different concentrations of the electrolytes KCl, KBr and NaCl.

Synthesis of Ag Nps@suc

The aqueous solution of HPC-Suc was mixed with $AgNO_3$ aqueous solution and exposed to sunlight. The color of solution started changing immediately after exposure to sunlight indicating formation of Ag Nps@suc. The synthesized Ag Nps@suc suspensions exhibited different colors at different sunlight exposure times. A photograph showing the color change upon exposure of the mixture to sunlight is presented in Figure 1.

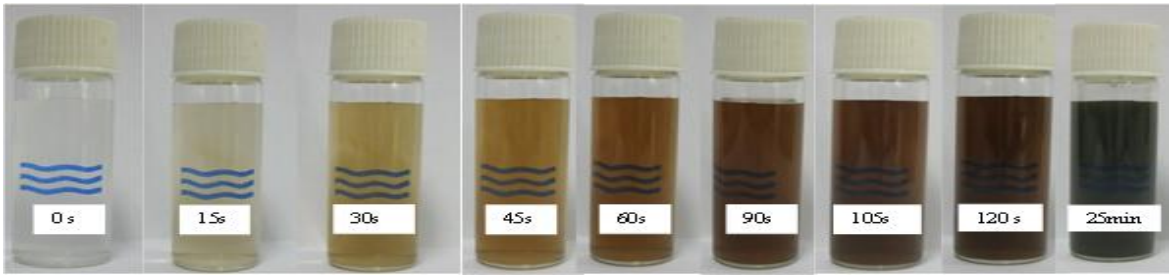

Figure 1. Photographs of mixture of HPC-Suc and Ag^+ solutions showing a change in color due to reduction of Ag^+ upon different time of exposure to sunlight

The change in color of these Ag Nps@suc suspensions upon exposure to sunlight is likely due to reduction of Ag^+ to Ag^0 forming hydroxypropyl cellulose succinate capped silver nanoparticles (Ag NPs@suc). Figure 2B shows the proposed scheme of synthesis of Ag Nps@suc by light induced reduction of Ag^+. The carboxylate groups of HPC-Suc are thought to reduce Ag^+ to Ag^0 (upon exposure to light) to form Ag Nps accompanied by decarboxylation of the reducing agent (Stankus et al., 2010). These succinate groups of HPC-Suc are thought to act as capping agents in addition to their role as a reducing agent.

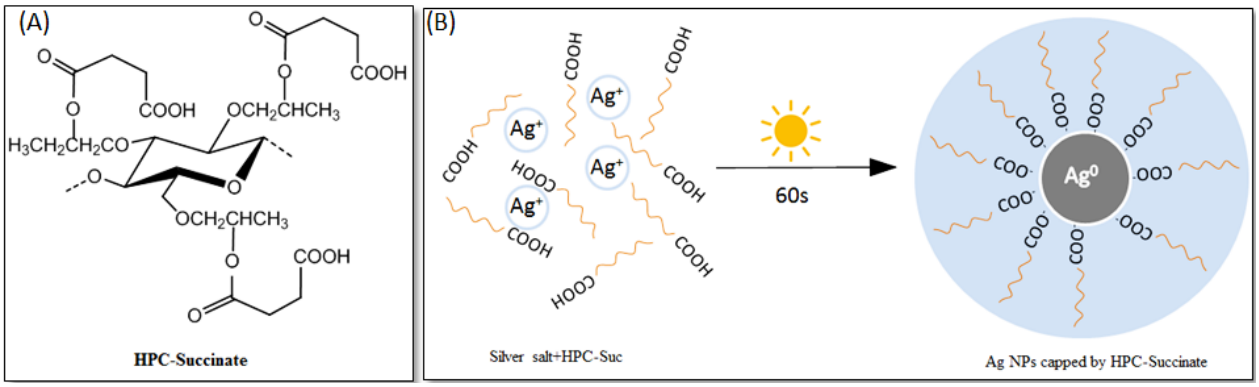

Figure 2. (A) Structure of HPC-Suc and (B) likely structure of Ag Nps-capped with HPC-Suc

Characterization of Ag Nps@suc

The UV-Vis, SEM-EDX, DLS and ZP, ATR-FTIR and nano-impacts were used for characterization of synthesized Ag Nps@suc. UV-Vis spectrometry showed that the collective oscillation of conduction electrons in Ag NPs@suc results in LSPR with a single and broad LSPR peak was observed in the range 411-452 nm confirming the synthesis of Ag Nps (Section S1, Figure S1) (Mulvaney, 1996). The size and morphological characterizations of Ag Nps@suc were determined by

SEM-EDX (Table 1). SEM images are provided in Section S2 in the Supplementary Information. Figure 3C shows the histogram for the distribution of AgNps@suc sizes determined by SEM. The Ag Nps were mostly spheroid shaped and a mean diameter value of 19.6 ± 6.8 nm was calculated (Figure S2A-D). Elemental EDX mapping (Figure S2 E-G) of Ag Nps@suc shows that Ag Nps are randomly dispersed throughout the Ag Nps@suc sample. The EDX elemental analysis also showed the presence of the elements (Ag, C and O) expected to be present in the Ag Nps@suc (Figure S3). To find out various functional groups present in HPC-Suc and Ag Nps@suc ATR-FTIR spectra of HPC, HPC-Suc and Ag Nps@suc were recorded as shown in Section S3 (Figure S4). The ATR-FTIR spectrum of HPC shows absorption bands at 3433, 2902 and 1160-1057 cm^{-1} indicating the presence of –OH, -CH_2- and C-O-H and C-O-C bonds, respectively. The appearance of absorption peaks in the FTIR spectrum of HPC-Suc at 1726, 1618, 1399, 1260 and 1140-1007 cm^{-1} due to C=O, COOH, C-O, C-O-H and C-O-C bonds, respectively is attributed to the successful esterification of of HPC to form HPC-Suc. The FTIR spectrum of Ag Nps@suc showed bands closely similar to those in FTIR spectrum of HPC-Suc. Retention of all these signals with the expected slight shift of frequency, in the ATR-FTIR spectrum of Ag Nps@suc is a strong evidence that HPC-Suc is present as capping agent of Ag in this study.The shifting of the C=O signal to 1724 cm^{-1}, -COOH signal to 1602 cm^{-1}, C-O signal to 1293 cm^{-1}, C-O-H, C-O-C signal to 1020-1057 cm^{-1} and the appearance of a 527-569 cm^{-1} signal due to Ag---O weak interactions in FTIR spectrum of Ag Nps@suc shows a success of reduction and capping of Ag^+ to form Ag Nps by HPC-Suc (Gupta et al., 2010; Shameli et al., 2012).

The ZP value measured for Ag Nps@suc (in water) was -31.8 ± 2.4 mV (Figure S5A). The higher and longer stability of nanoparticles is due to relatively high values of negative ZP. The size of Ag Nps@suc was also measured by DLS and the z-average was found to be 19.7 ± 1.7 nm (Section S4, Table 1, Figure S5 B).

In addition to SEM and the DLS measurements, the size of Ag Nps@suc was also investigated using nano-impacts experiments. Nanoparticle-electrode impacts embraces APC and record single events through the generation of electrochemical signal by a redox reaction taking place on a nanoparticle. The oxidation of silver nanoparticles is a model of the well characterized system and the electrode reaction in this case can be described as (Allerston and Rees 2018; Sokolov et al., 2017; Stevenson and Tschulik, 2017):

$$Ag_N \rightarrow N\,Ag^+ + Ne^- \qquad (1)$$

In the present study, a 12 pM solution of Ag Nps@suc in 20 mM KCl was subjected to APC measurement. Ag Nps@suc diffuse through the solution under Brownian movement and collide with the carbon microelectrode of 33 µm diameter held at a suitable oxidising potential (in this case +0.8V). Oxidation of Ag Np takes place from Ag^0 to Ag^+ (likely resulting in the formation of AgCl) (Ngamchuea

et al., 2017b) generating a current 'spike'. These spikes can be recorded as current-time transients or through a cyclic voltammogram. The later type of measurement is helpful for knowing the potential at which the potential oxidation onset. The area under a single nano-impact spike corresponds to the total charge required for the oxidation of the colliding Ag Nps. The size of the later can be estimated by Eq. 2 which assumes that silver nanoparticle is spherical and is fully oxidized (Little et al., 2018):

$$r = \sqrt[3]{\frac{3MQ}{4\pi Fz\rho}} \quad (2)$$

where r is the radius of Ag Nps@suc, M is the atomic mass of silver (107.9 g mol^{-1}), Q is the charge calculated from area under each 'spike', z is the number of electrons transferred per oxidised silver atom, F is the Faraday constant (96485 C mol^{-1}), and ρ is the density of bulk silver (10.5×10^{6} g m^{-3}). Figure 3A displays a typical current-time transient.

In addition to nano-impact studies carried out using chronoamperometry at a fixed potential, cyclic voltametry is also be employed to calculate the diameter of Ag Nps@suc. In the present case, 12 pM solution of Ag Nps@suc in 20 mM KCl was used and voltammograms were recorded as soon as the solution was prepared using a three electrode system containing carbon micro-electrode of 33 µm diameter at a scan rate of 50 mV s^{-1}. These voltammograms were analysed and the area under each spike was calculated again. Figure 3B shows a typical voltammogram. The area under each spike is related to charge transferred during a single nanoparticle oxidation event. This area is divided by scan rate to get charge, Q. The charge calculated from chronoamperometric and cyclic voltametric spikes is combined. Eq. 2 is used to get the radius and hence diameter or size of the Ag Np. In the present study total of 1036 spikes from 8 scans were analysed and a mean diameter of Ag Nps@suc was calculated to be 16.7 ± 3.3 nm. This value is in a good agreement with results obtained from SEM and DLS as shown in Table 1. Figure 3C shows the distribution of AgNps@suc sizes obtained independently from nano-impacts and SEM; good agreement is apparent. SEM and impacts assume particles as spheres. Table 1 shows the characteristics parameters for the as synthesized silver nanoparticles.

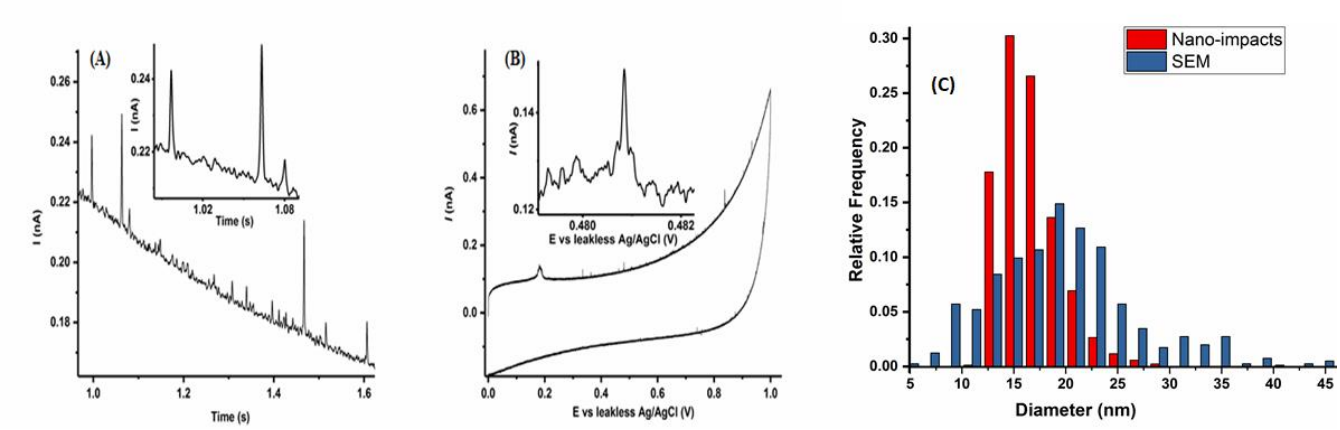

Figure 3. (A) Chronoamperogram at E= +0.8 V *vs* leakless Ag/AgCl (inset depicts the enlarged chronoamperogram) (B) Cyclic voltammogram at scan rate 50 mVs^{-1} (inset depicts the enlarged voltammogram) showing nano-impact spikes of 12 pM Ag Nps@suc in 20 mM KCl using 33µm carbon microdisc electrode, leakless Ag/AgCl reference electrode and platinum counter electrode and (C) The histograms show the distribution of AgNps@suc sizes calculated from the charge of nano-impact spikes of 12 pM Ag Nps@suc oxidation events in 20 mM KCl electrolyte solutions compared with sizes determined by SEM

Table 1. Sizing results of the as-synthesized Ag Nps@suc

Method	Diameter (nm)
Nano-impacts	16.7±3.3
SEM	19.8±6.8
DLS (z-ave)	19.7±1.7

Determination of the concentration of Ag Nps@suc in a suspension

On the basis of the diameter (ca. 20 nm) of Ag Nps@suc determined by SEM, the concentration of a Ag Nps suspension was estimated by UV-Vis and was found to be 189 ± 6.5 pM using the procedure of Ngamchuea and co-workers (Ngamchuea et al., 2017). Details are available in Section S5 of the Supplementary Information.

Stability study of Ag Nps in K_2SO_4 (citrate *vs* succinate capping)

The stability of the Ag Nps@suc was studied in K_2SO_4 electrolyte using UV-Vis and nano-impacts measurements and compared with the stability of Ag Nps@cit. Two different concentrations of the synthesized Ag Nps@suc (4 pM and 12 pM) were examined in three different concentrations (2 mM,

20 mM and 100 mM) of K_2SO_4 using UV-Vis and the results were compared with those from Ag Nps@cit in order to provide insights into the relative clustering rates of the Ag Nps@suc and Ag Nps@cit at different concentrations of K_2SO_4. Besides UV-Vis, the clustering state of the Ag Nps was also investigated using the nano-impact technique in 100 mm K_2SO_4 where the term 'clustering' covers both agglomeration and aggregation.

Stability study of Ag Nps using UV-Vis

A comparison of the stability of succinate and citrate capped silver nanoparticles in different concentrations of K_2SO_4 was made to show that colloidal suspensions of Ag Nps@suc are significantly more stable than those of Ag Nps@cit. Figure 4 shows representative UV-Vis spectra of 12 pM silver nanoparticles (Ag Nps@suc and Ag Nps@cit) in 100 mM K_2SO_4 recorded at different time intervals after making solutions. There is a negligible decrease in absorbance (Figure 4A) with a slight shift in λ_{max} from 428.5 nm to 419.5 nm for Ag Nps@suc after 24 h. No change in peak shape is observed even after 24 h for Ag Nps@suc. On the other hand, for the Ag Nps@cit, a relatively broader peak appeared with a decrease in λ_{max} from 397.5 nm to 390 nm immediately after adding the salt (100 mM K_2SO_4) and importantly a shoulder at around 570 nm was observed in the peak. For the Ag Nps@cit, there was a significant change in the LSPR peak shape and peak height between 1 h and 24 h. The reason behind these losses might be a rapid clustering of Ag Nps@cit. Figure 5A shows a plot of absorbance against time of Ag Nps@suc and Ag Nps@cit (12 pM) in 100 mM K_2SO_4. It is clear from Figure 4B that the absorbance for Ag Nps@cit in 100 mM K_2SO_4 decreased markedly after 24 h, suggesting complete clustering of the Nps. About half of the peak decay was observed within seconds immediately after adding the electrolyte. On the contrary, Ag Nps@suc showed a little clustering as can be evidenced from only a slight decrease in absorbance over 24 h. Similar results were obtained at lower concentration of Ag Nps (4 pM of Ag Nps@suc and Ag Nps@cit in 100 mM K_2SO_4) where Ag Nps@cit lost almost one-third of the peak absorbance only within 1 h while there was only a small absorbance loss in case of Ag Nps@suc after 24 h (Figure S6 B, Table S1). This negligible decrease in absorbance in case of succinate capped silver nano-particles at high ionic strength shows that Ag Nps@suc are usefully more stable than Ag Nps@cit. The decrease in absorbance of the Ag Nps in the electrolyte is attributed to clustering of the nanoparticles.

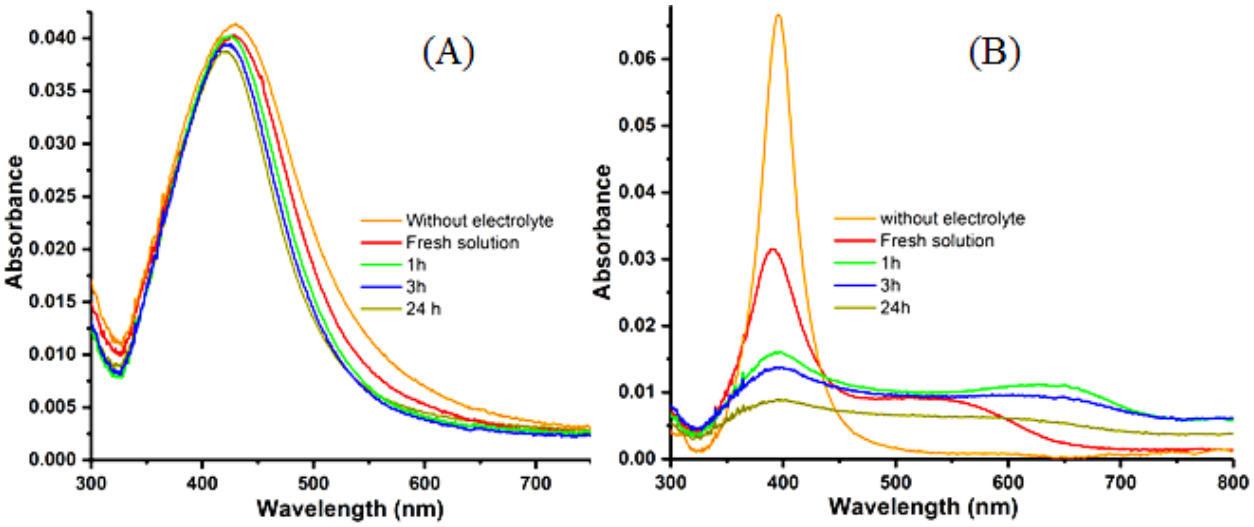

Figure 4. Representative UV-Vis spectra of (A) 12 pM Ag Nps@suc (B) 12 pM Ag Nps@cit in 100 mM K_2SO_4 over a period of 24 h. Orange lines in both spectra represent 12 pM Ag Nps without the electrolyte

At lower ionic strengths of the electrolyte (20 mM K_2SO_4) there was only a negligible loss of peak absorbance for 12 pM Ag Nps@suc. On the other hand, for 12 pM Ag Nps@cit, about half of the Ag Nps were clustered which can be seen from half of the decay in absorbance to half (Figure S6 B). For 4 pM concentration of Ag Nps in 20 mM K_2SO_4,there was almost a complete loss in absorbance for Ag Nps@cit after 24 h while for Ag Nps@suc, there was a slight decay in absorbance after the same time (Figure S6 A). All these results show that Ag Nps@suc are more stable than Ag Nps@cit. Ag Nps@suc showed a mean λ_{max} value of 425.5 ± 6.0 nm for all the concentration of Ag Nps@suc in all the studied concentrations of electrolytes. The wavelength of maximum absorbance (λ_{max}) in case of Ag Nps@cit in all concentrations of K_2SO_4 was 395.5 ± 2.0 nm.

The analyses of the absorbance data in the other concentrations of electrolyte K_2SO_4 are presented in Figure S6 and Table S1.

Stability study of Ag Nps using electrochemical Nano-impacts

The clustering of Nps in a specific liquid environment can also be investigated using the nano-impact method (Ellison et al., 2013; Jiao et al., 2017; Kätelhön et al., 2017; Rees et al., 2011; Shimizu et al., 2017). The clustering of silver nanoparticles (12 pM) in a solution containing 100 mM K_2SO_4 was studied *via* impact-based APC over a period of 3 h. Figure S7 displays representative chronoamperograms showing nano-impact spikes of 12 pM Ag Nps@suc and Ag Nps@cit in 100 mM K_2SO_4 for a fresh solution of silver nanoparticles and a solution aged for 1 h and 3 h. The charge needed for quantitative

oxidation of Ag Nps@suc and Ag Nps@cit is measured by integrating the area of nano-impact spike which is obtained when a nanoparticle collides with a micro-electrode (Suherman et al., 2018; Zampardi et al., 2018; Zhou et al., 2012). This charge is then related to the number of atoms present in the nanoparticle or nanoparticle clusters. This number of atoms is related to the number of nanoparticle monomers which in turn gives the size of each impacting clusters. Figure 5 B shows the mean size of 12 pM each of Ag Nps@suc and Ag Nps@cit in 100 mM K_2SO_4 plotted against time. It is clear from the plot that the mean size in case of Ag Nps@cit increases from 26.7 ± 8.9 nm to 35.8 ± 7.5 nm over a period of 3 h while in case of Ag Nps@suc, the size almost remains constant (17.4 ± 3.2 nm to 18.3 ± 5.1 nm). Although, both types of the Ag Nps have almost the same size (~20 nm) in stock solution, Ag Nps@cit shows a larger size (26.7 ± 8.9 nm) after the very few seconds of making the solution due to the rapid clustering of Ag Nps@cit immediately after adding the K_2SO_4 salt. This confirms the higher stability of Ag Nps@suc over Ag Nps@cit. This sudden clustering in case of Ag Nps@cit is also supported by the sudden decrease in peak absorbance in UV-Vis immediately after adding electrolyte (Figure 4 B). These clusters on colliding with the micro-electrode cause a greater oxidative charge, as they are larger. This can also be evidenced by a significant increase in duration of spike in the case of Ag Nps@cit (Figure S7 A). While in case of Ag Nps@suc no appreciable increase in size is observed showing negligible clustering in these nanoparticles.

Figure S8 B shows the frequency of spikes of 12 pM Ag Nps@suc and Ag Nps@cit in 100 mM K_2SO_4 as a function of time. The clustering in case of Ag Nps@cit can also be evidenced by a prominent reduction in frequency of spikes with time over a period of 3 h (Figure S8 B). According to the Stokes-Einstein equation (Einstein, 1905), the clustered nanoparticles will have a decreased diffusion coefficient which results in a decreased number of observable impacts at microelectrode and hence less frequency. The decrease in frequency of spikes in case of Ag Nps@cit can also be attributed to the fact that number of observed impacts decrease due to the decrease in number of the diffusing species due to clustering of Nps.

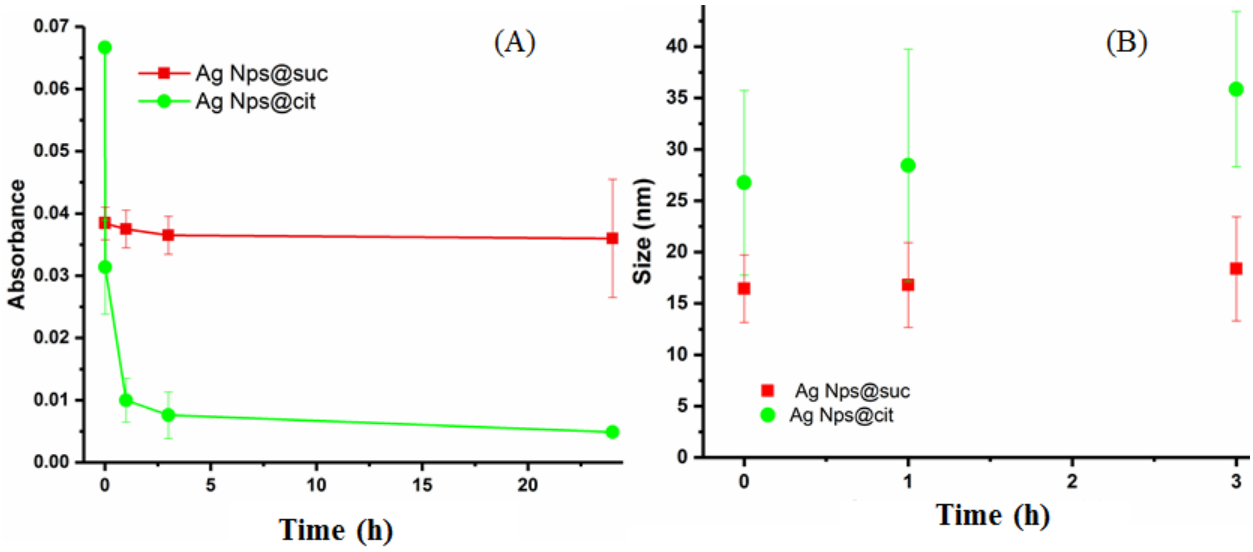

Figure 5. Absorbance (A) and mean size by nano-impact (B) as a function of time of Ag Nps@suc and Ag Nps@cit (12 pM) in 100 mM K_2SO_4

Effect of different electrolytes on clustering

The stability of the Ag Nps@suc was also studied in three other different electrolytes (KCl, KBr and NaCl) using UV-Vis and results are compared with those from Ag Nps@cit. Two different concentrations of Ag Nps solutions (4 pM and 12 pM) are studied in three different concentrations (2 mM, 20 mM and 100 mM) of all the three electrolytes.

UV-Vis spectra in different electrolytes

In order to have an insight into the stabilities of Ag Nps@suc and Ag Nps@cit, clustering of Ag Nps was also investigated in three more electrolytes (KCl, KBr and NaCl). UV-Vis spectra of different concentrations of both types of Ag Nps in different concentrations of electrolytes were recorded over a period of 24 h. Figure 6 shows representative UV-Vis spectra of fresh solutions of 12 pM silver nanoparticles (Ag Nps@suc and Ag Nps@cit) in 20 mM KCl at different time. The λ_{max} is shifted from 408.5 nm to 398.5 nm for Ag Nps@suc and from 395 nm to 391 nm for the Ag Nps@cit after 24 h (Figure 5). The λ_{max} for Ag Nps@cit in all electrolytes was 394.5 ± 4 nm. For Ag Nps@suc, the value of λ_{max} in KCl, KBr and NaCl was found to be 406 ± 6 nm. It is clear from the spectra (Figure 6), that the absorbance for Ag Nps@cit in KCl significantly decreases over time. The reason of the decrease in absorbance in Ag Nps@cit may be attributed to clustering of particles in the presence of electrolyte. Clustering of Nps is normally evidenced by a decrease in absorbance in UV spectra. On the contrary, Ag Nps@suc shows a small increase in absorbance over 24 h. Increase in absorbance of the Ag Nps in the

presence of electrolyte might be due to two reasons (i) formation of more Ag Nps due to reduction of any interested silver ions in suspension (ii) a relatively big agglomerate of silver nanoparticles disintegrate to yield more isolated particles. The first possibility can be excluded because we do not expect any silver ions after centrifugation and washing. So, the second reason could be the most probable. This hypothesis is also supported by the fact that a decrease in λ_{max} (~10 nm in all electrolytes) is observed for Ag Nps@suc solution in KCl after 24 h.

Results of analysis of the absorbance data for different concentrations of Ag Nps in different concentrations of different electrolytes are displayed in Table S2 and Figure S9. In case of 12 pM and 4 pM concentrations of Ag Nps in 20 mM and 2 mM concentrations of all the three electrolytes, the absorbance in case of Ag Nps@suc does not show any significant decrease over the period of 24 h (except in 20 mm KBr where a greater decrease in absorbance was observed as can be seen from Figure S9 D). For instance, in 20 mM NaCl, the Ag Nps@suc showed no decrease in peak absorbance after 24 h which suggested negligible clustering in these Nps and thus excellent stability. However, for the Ag Nps@cit, a greater decrease in peak absorbance in 20 mM of NaCl was found after 24 h showing higher clustering of these Nps. A complete decay in peak absorbance for Ag Nps@cit was observed in 20 mM KBr after 24 h (Figure S9 C), which could be due to significant clustering in suspension. A higher decrease in absorbance for Ag Nps@suc was observed in KBr electrolyte after 24 h but it was still less than in the case of Ag Nps@cit showing their higher stability. In case of higher ionic strength of electrolytes (100 mM), both types of Ag Nps (Ag Nps@suc and Ag Nps@cit) were almost completely clustered after 24 h but the clustering rate in both types of Ag Nps was found to be different. For instance, a very rapid loss in peak absorbance was observed for Ag Nps@cit after 1 h while in case of Ag Np@suc, there was only one-third loss in peak absorbance within the same time (Figure S9 A). This rapid decrease in absorbance after 1 h in case of Ag Nps@cit may be due to the fact that these Nps are charge stabilized while steric stabilization of Ag Nps@suc might be a reason for comparatively slow rates of clustering in these Nps. The observed significant differences in the decrease in absorbance at different ionic strengths of different electrolytes are due to preferential absorption of a specific ion which causes clustering and alters surface chemistry.

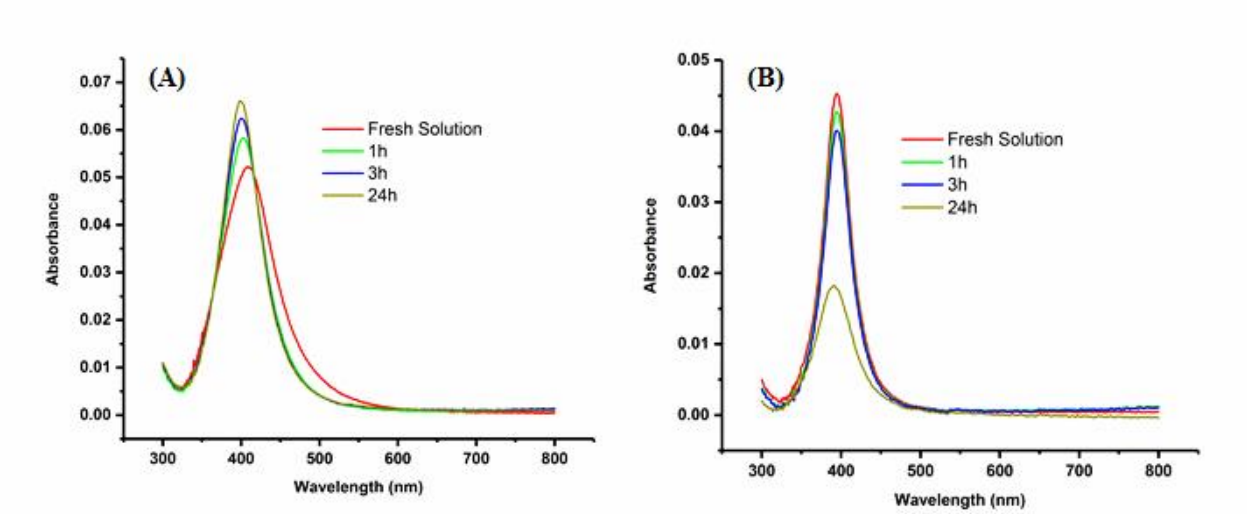

Figure 6. Representative UV-Vis spectra of (A) 12 pM Ag Nps@suc (B) 12 pM Ag Nps@cit of diameter 20 nm in 20 mM KCl over a period of 24 h

From the above results we conclude that Ag Nps@suc are more stable than Ag Nps@cit. This enhanced stability might be attributed to the inclusion of HPC polymer in the capping agent which acts as a substrate for linking carboxylic acid to the Ag Nps. Additionally, the polymer chain might help in forming uniformly capped Ag Nps thus improving the stability.

Conclusions

Stable Ag Nps@suc of diameter ~20 nm were successfully fabricated using a simplified and green strategy. LSPR peak of synthesized Ag Nps@suc was observed in the range 411-452 nm. SEM-EDX images showed that the Ag Nps were mostly randomly dispersed spheroid containing elements Ag, C and O. Sizing of NPs using nanoparticle collision method was consistent with SEM and DLS results. UV-Vis spectrometry and nano-impact studies in high concentration of K_2SO_4 showed excellent stability of developed Ag Nps@suc as compared with the widely employed Ag Nps@cit. The high stability of Ag Nps@suc is consistent with a high negative value of ZP (-31.8 ± 2.4 mV) for these nanoparticles. The high stability of such Ag Nps@suc, which are synthesized *via* a simple method, could encourage their use as a potential stable catalysts and as possible carriers in drug delivery.

Acknowledgments

A. Abbas thanks the Punjab Higher Education Commission (PHEC), Pakistan (Grant No. PHEC/A&R/FPDF/1-18/2017) for a post-doctoral grant. H. M. A. Amin thanks the German Research Foundation DFG for funding (Grant No. AB 702/1-1). M.A is a recipient of Foreign Post-Doctoral Fellowships Program FY 2016-2017 funded by Punjab Higher Education Commission (PHEC/A&R/FPDF/1-15/2017), Government of Punjab, Pakistan.

Conflict-of-Interest Statement

There are no conflicts of interest to declare.

References

Abbas, A., Hussain, M.A., Amin, M., Tahir, M.N., Jantan, I., Hameed, A., & Bukhari, S.N.A. (2015). Multiple cross-linked hydroxypropylcellulose–succinate–salicylate: prodrug design, characterization, stimuli responsive swelling–deswelling and sustained drug release. RSC Advances, 5, 43440-43448.

Abdelgawad, A.M., El-Naggar, M.E., Eisa, W.H., & Rojas, O.J. (2017). Clean and high-throughput production of silver nanoparticles mediated by soy protein via solid state synthesis. Journal of Cleaner Production, 144, 501-510.

Afshinnia, K., Sikder, M., Cai, B., & Baalousha, M. (2017). Effect of nanomaterial and media physicochemical properties on Ag NM aggregation kinetics. Journal of Colloid and Interface Science, 487, 192-200.

Allerston, L.K., & Rees, N.V. (2018). Nanoparticle impacts in innovative electrochemistry. Current Opinion in Electrochemistry, 10, 31-36.

Amin, H.M.A., Baltruschat, H., Wittmaier, D., & Friedrich, K.A. (2015). A highly efficient bifunctional catalyst for alkaline air-electrodes based on a Ag and Co_3O_4 hybrid: RRDE and online DEMS insights. Electrochimica Acta, 151, 332-339.

Amin, H.M.A., Bondue, C.J., Eswara, S., Kaiser, U., & Baltruschat, H. (2017). A carbon-free Ag–Co_3O_4 composite as a bifunctional catalyst for oxygen reduction and evolution: spectroscopic, microscopic and electrochemical characterization. Electrocatalysis, 8, 540-553.

Baalousha, M. (2017). Effect of nanomaterial and media physicochemical properties on nanomaterial aggregation kinetics. NanoImpact, 6, 55-68.

Banach, M., & Pulit-Prociak, J. (2017). Proecological method for the preparation of metal nanoparticles. Journal of Cleaner Production, 141, 1030-1039.

Bastús, N.G., Merkoçi, F., Piella, J., & Puntes, V. (2014). Synthesis of highly monodisperse citrate-stabilized silver nanoparticles of up to 200 nm: kinetic control and catalytic properties. Chemistry of Materials, 26, 2836-2846.

Batchelor-McAuley, C., Ellison, J., Tschulik, K., Hurst, P.L., Boldt, R., & Compton, R.G. (2015). *In situ* nanoparticle sizing with zeptomole sensitivity. Analyst, 140, 5048-5054.

Einstein, A. (1905). On the movement of small particles suspended in stationary liquids required by molecular-kinetic theory of heat. Annalen der Physik, 17, 549−560.

Ellison, J., Tschulik, K., Stuart, E.J.E., Jurkschat, K., Omanovic´, D., Uhlemann, M., Crossley, A., & Compton, R.G. (2013). Get more out of your data: a new approach to agglomeration and aggregation studies using nanoparticle impact experiments. ChemistryOpen, 2, 69-75.

Gupta, K., Jana, P.C., & Meikap, A.K. (2010). Optical and electrical transport properties of polyaniline–silver nanocomposite. Synthetic Metals, 160, 1566-1573.

Hayward, R.C., Saville, D.A., & Aksay, I.A. (2000). Electrophoretic assembly of colloidal crystals with optically tunable micropatterns. Nature, 404, 56-59.

Huynh, K.A., & Chen, K.L. (2011). Aggregation kinetics of citrate and polyvinylpyrrolidone coated silver nanoparticles in monovalent and divalent electrolyte solutions. Environmental Science and Technology, 45, 5564-5571.

Jang, M.-H., Bae, S.-J., Lee, S.-K., Lee, Y.-J., & Hwang, Y.S. (2014). Effect of material properties on stability of silver nanoparticles in water. Journal of Nanoscience and Nanotechnology, 14, 9665-9669.

Jiao, X., Sokolov, S.V., Tanner, E.E.L., Young, N.P., & Compton, R.G. (2017). Exploring nanoparticle porosity using nano-impacts: platinum nanoparticle aggregates. Physical Chemistry Chemical Physics, 19, 64-68.

Kätelhön, E., Sokolov, S.V., Bartlett, T.R., & Compton, R. G. (2017). The role of entropy in nanoparticle agglomeration. Chemphyschem, 18 51-54.

Kätelhön, E., Tanner, E. E. L., Batchelor-McAuley, C., & Compton, R.G. (2016). Destructive nano-impacts: What information can be extracted from spike shapes? Electrochimica Acta, 199, 297-304.

Khan, M., Khan, S.T., Khan, M., Adil, S.F., Musarrat, J., Al-Khedhairy, A.A., Al-Warthan, A., Siddiqui, M.R.H., & Alkhathlan, H.Z. (2014). Antibacterial properties of silver nanoparticles synthesized using *Pulicaria glutinosa* plant extract as a green bioreductant. International Journal Nanomedicine, 9, 3551-3565.

Korshed, P., Li, L., Ngo, D.-T., & Wang, T. (2018). Effect of storage conditions on the long-term stability of bactericidal effects for laser generated silver nanoparticles. Nanomaterials, 8, 1-12.

Lees, J.C., Ellison, J., Batchelor-McAuley, C., Tschulik, K., Damm, C., Omanovic, D., & Compton, R.G. (2013). Nanoparticle impacts show high-ionic-strength citrate avoids aggregation of silver nanoparticles. ChemPhysChem, 14, 3895-3897.

Little, C.A., Li, X., Batchelor-McAuley, C., Young, N.P., & Compton, R.G. (2018). Particle-electrode impacts: Evidencing partial versus complete oxidation via variable temperature studies. Journal of Electroanalytical Chemistry, 823, 492-498.

Luo, C., Zhang, Y., Zeng, X., Zeng, Y., & Wang, Y. (2005). The role of poly(ethylene glycol) in the formation of silver nanoparticles. Journal of Colloids and Interface Science, 288, 444-448.

Mfouo-Tynga, I., El-Hussein, A., Abdel-Harith, M., & Abrahamse, H. (2014). Photodynamic ability of silver nanoparticles in inducing cytotoxic effects in breast and lung cancer cell lines. International Journal of Nanomedicine, 9, 3771-3780.

Mulvaney, P. (1996). Surface plasmon spectroscopy of nanosized metal particles. Langmuir, 12, 788-800.

Ngamchuea, K., Batchelor-McAuley, C., Sokolov, S.V., & Compton, R.G. (2017). Dynamics of silver nanoparticles in aqueous solution in the presence of metal ions. Analytical Chemistry, 89, 10208-10215.

Ngamchuea, K., Clark, R.O.D., Sokolov, S.V., Young, N.P., Batchelor-McAuley, C., & Compton, R.G. (2017b). Single oxidative collision events of silver nanoparticles: understanding the rate-determining chemistry. Chemistry. A European Journal, 23, 16085-16096.

Peijnenburg, W.J.G.M., Baalousha, M., Chen, J., Chaudry, Q., Von der Kammer, F., Kuhlbusch, T.A.J., Lead, J., Nickel, C., Quik, J.T.K., Renker, M., Wang, Z., & Koelmans, A.A. (2015). A review of the properties and processes determining the fate of engineered nanomaterials in the aquatic environment. Critical Reviews in Environmental Science and Technology, 45, 2084-2134.

Raveendran, P., Fu, J., & Wallen, S.L. (2003). Completely "green" synthesis and stabilization of metal nanoparticles. Journal of the American Chemical Society, 125, 13940-13941.

Rees, N.V., Zhou, Y.-G., & Compton, R.G. (2011). The aggregation of silver nanoparticles in aqueous solution investigated via anodic particle coulometry. ChemPhysChem, 12, 1645-1647.

Richard, D., Couves, J.W., & Thomas, J.M. (1991). Structural and electronic properties of finely-divided supported Pt-group metals and bimetals. Faraday Discussions, 92, 109-119.

Shamaila, S., Sajjad, A.K.L., Ryma, N.-ul-A., Farooqi, S.A., Jabeen, N., Majeed, S., & Farooq, I. (2016). Advancements in nanoparticle fabrication by hazard free eco-friendly green routes. Applied Materials Today, 5, 150-199.

Shameli, K., Ahmad, M.B., Jazayeri, S.D., Sedaghat, S., Shabanzadeh, P., Jahangirian, H., Mahdavi, M., & Abdollahi, Y. (2012). Synthesis and characterization of polyethylene glycol mediated silver nanoparticles by the green method. International Journal of Molecular Sciences, 13, 6639-6650.

Shimizu, K., Sokolov, S.V., Young, N.P., & Compton, R.G. (2017). Particle-impact analysis of the degree of cluster formation of rutile nanoparticles in aqueous solution. Physical Chemistry Chemical Physics, 19, 3911-3921.

Shipway, A.N., Katz, E., & Willner, I. (2000). Nanoparticle arrays on surfaces for electronic, optical, and sensor applications. ChemPhysChem, 1, 18-52.

Sokolov, S.V., Eloul, S., Kätelhön, E., Batchelor-McAuley, C., & Compton, R.G. (2017). Electrode–particle impacts: a users guide. Physical Chemistry Chemical Physics, 19, 28-43.

Stankus, D.P., Lohse, S.E., Hutchison, J.E., & Nason, J.A. (2011). Interactions between natural organic matter and gold nanoparticles stabilized with different organic capping agents. Environmental Science & Technology, 45, 3238-3244.

Stevenson, K.J., & Tschulik, K. (2017). A materials driven approach for understanding single entity nano impact electrochemistry. Current Opinion in Electrochemistry, 6, 38-45.

Stuart, E.J.E., Rees, N.V., Cullen, J.T., & Compton, R.G. (2013). Direct electrochemical detection and sizing of silver nanoparticles in seawater media. Nanoscale, 5, 174-177.

Suherman, A.L., Zampardi, G., Kuss, S., Tanner, E.E.L., Amin, H.M.A., Young, N.P., & Compton, R.G. **(**2018). Understanding gold nanoparticle dissolution in cyanide-containing solution *via* impact-chemistry. Physical Chemistry Chemical Physics, 20, 28300-28307.

Xie, J., Lee, J.Y., Wang, D.I.C., & Ting, Y.P. (2007). Silver nanoplates: from biological to biomimetic synthesis. ACS Nano, 1, 429-439.

Zampardi, G., Thöming, J., Naatz, H., Amin, H.M.A., Pokhrel, S., Mädler, L., & Compton, R.G. (2018). Electrochemical behavior of single CuO nanoparticles: implications for the assessment of their environmental fate. Small, 14, 1801765.

Zhao, Q., Duan, R., Yuan, J., Quan, Y., Yang, H., & Xi, M. (2014). A reusable localized surface plasmon resonance biosensor for quantitative detection of serum squamous cell carcinoma antigen in cervical cancer patients based on silver nanoparticles array. International Journal Nanomedicine, 9, 1097-1104.

Zhou, Y.-G., Rees, N.V., Pillay, J., Tshikhudo, R., Vilakazi, S., & Compton, R.G. (2012). Gold nanoparticles show electroactivity: counting and sorting nanoparticles upon impact with electrodes. Chemical Communications, 48, 224-226.